Phys. Status Solidi C **13**, No. 10–12, 750–755 (2016) / **DOI** 10.1002/pssc.201600038

physica status solidi c
www.pss-c.com
current topics in solid state physics

Simulation of the proton implantation process in silicon

Martin Faccinelli[*,1], Moriz Jelinek[2], Thomas Wuebben[2], Johannes G. Laven[3], Hans-Joachim Schulze[3], and Peter Hadley[1]

[1] Graz University of Technology, Institute of Solid State Physics, Graz 8010, Austria
[2] Infineon Technologies Austria AG, Villach 9500, Austria
[3] Infineon Technologies AG, Neubiberg 85579, Germany

Received 2 May 2016, revised 10 June 2016, accepted 25 June 2016
Published online 22 July 2016

Keywords proton implantation, defect complexes, process simulation, diffusion-reaction-dissociation

[*] Corresponding author: e-mail mfaccinelli@tugraz.at, Phone: +43-316-8738960, Fax: +43-316-8738466

Proton implantation is one of many processes used to adjust the electronic and mechanical properties of silicon. Though the process has been extensively studied, it is still not clear which exact defects are formed and what their concentration profiles are. In this article, a simulation method is presented, which provides a better understanding of the implantation process. The simulation takes into account the diffusion of mobile point defects and their reactions to defect complexes, as well as the dissociation of defect complexes. Concentration profiles for a set of defect complexes after an implantation at 400 keV and a dose of 5×10^{14} H^+cm^{-2} are presented.

1 Introduction The implantation of protons in silicon is used for several purposes. Small implantation doses are used to fine tune the minority charge carrier lifetime in power electronic devises [1]. Medium doses result in the production of hydrogen related donors and are used for generating n-type regions in the sample [2]. When a high dose of protons is implanted into silicon, plate-like defects are generated which are used in the Smart Cut process to cleave thin slices off a silicon wafer [3].

When protons are implanted into crystalline silicon, a small fraction of their energy is used to knock out silicon atoms from lattice sites. This generates a high concentration of vacancies (V) and interstitial silicon atoms (I). Once all their kinetic energy is dissipated, the implanted protons come to rest in a region called the projected range or implantation depth. The generated point defects diffuse according to

$$\frac{\delta c}{\delta t} = D\nabla^2 c, \tag{1}$$

where c is the defect concentration and D is the diffusivity. Here we assume that the temperature dependence of the diffusivity can be described by an Arrhenius equation

$$D = D_0 e^{-\frac{E_{A,diff}}{k_B T}}, \tag{2}$$

where D_0 is the diffusion pre-factor, $E_{A,diff}$ is the activation energy and k_B is Boltzmann's constant. In the case of proton implantation, the concentration of defects is so low that immediate reactions between the defects are unlikely. Instead, two point defects, A and B, diffuse through the lattice until the distance between them decreases to a critical range called the capture radius r_c where they react to form a defect complex AB:

$$A + B \underset{kd}{\overset{kp}{\rightleftharpoons}} AB. \tag{3}$$

Here, kp is the reaction rate and kd is the dissociation rate. As the defect concentrations are small (ppm), the reaction rate kp is limited by the diffusion of two reaction partners towards the point where they eventually react. This is referred to as a diffusion limited reaction of second order and can be calculated from the diffusivities D_A and D_B of the two point defects and r_c as described, e.g. in Refs. [4,5]:

$$kp = 4\pi r_c (D_A + D_B). \tag{4}$$

The vacancies and interstitials generated by the impinging protons can either react with defects of the same kind to

form clusters (I_n, V_n), or react with each other and hence, recombine to a silicon atom on a lattice site. This recombination process can also be indirect, when an interstitial silicon atom reacts with a vacancy complex or a vacancy reacts with an interstitial complex as described in Eqs. (5).

$$\begin{aligned} V_n + V_m &\rightleftharpoons V_{n+m} \\ I_n + I_m &\rightleftharpoons I_{n+m} \\ I + V &\rightleftharpoons \text{(recombination)} \\ I_n + V_{m<n} &\rightleftharpoons I_{n-m} \\ V_n + I_{m<n} &\rightleftharpoons V_{n-m} \end{aligned} \tag{5}$$

Apart from the point defects generated and introduced by the proton implantation (V, I and H) the substrate material already contains impurities such as oxygen, carbon and dopant atoms (usually boron or phosphorous). While the preferential lattice site of oxygen is on an interstitial position, carbon and dopants tend to occupy substitutional lattice sites (e.g. C_s, B_s). Substitutional defects can react with silicon interstitials, hence, exchanging the lattice site, and becoming interstitial defects. Interstitial defects, on the other hand, can react with vacancies resulting in a substitutional defect. Both reactions combined can be seen as an indirect recombination of V and I. On the other hand, defects can also react with silicon interstitials or vacancies to form complexes. These complexes can further be the location of indirect recombination. These reactions are described by Eqs. (6).

$$\begin{aligned} C_s + I &\rightleftharpoons C_i \\ C_i + V &\rightleftharpoons C_s \\ O + I &\rightleftharpoons IO \\ IO + V &\rightleftharpoons O \end{aligned} \tag{6}$$

During the implantation the intrinsic point defects also react with vacancies forming defect complexes such as VO, also called the A-center. Many defect complexes are possible which can include several different kinds of point defects such as VOH, C_iOH or C_iOI. The defect complexes which are formed can also dissociate. This may in turn be described by a temperature activated process (see Refs. [6, 7]):

$$kd = f_A e^{-\frac{E_{A,diss}}{k_B T}}, \tag{7}$$

where kd is the dissociation rate, f_A is the attempt frequency and $E_{A,diss}$ is the activation energy for the dissociation process.

Depending on the implantation conditions, as well as on the parameters of the subsequent anneal, the concentration and the diffusion of the different defect complexes can vary strongly. This goes along with dramatic changes of the electronic and mechanical properties of the material. Figures 1 and 2 show measurements of proton implanted silicon samples using Spreading Resistance Profiling (SRP) for measuring electrically active defects and Transmission Electron Microscopy (TEM) for visualizing extended plate-like defects. Upon changing the implantation or annealing parameters, it is possible to measure how the mechanical and electrical properties are changed. However, it is not always possible to associate which microscopic defects are responsible for these changes. There is no experimental technique capable of measuring the concentrations and the distributions of the defects at the apparent low concentrations. Thus, it is difficult to assign changes in the electrical and mechanical properties to specific defects. The distribution of the hydrogen and the primary damage which is caused in the material during an implantation process can be calculated using Monte Carlo simulations such as SRIM [8, 9]. While such simulations provide a lot of information about the interaction of single particles with the substrate, they do not account for the subsequent diffusion and reactions of the defects which are produced. In this work we present a technique which takes this into account.

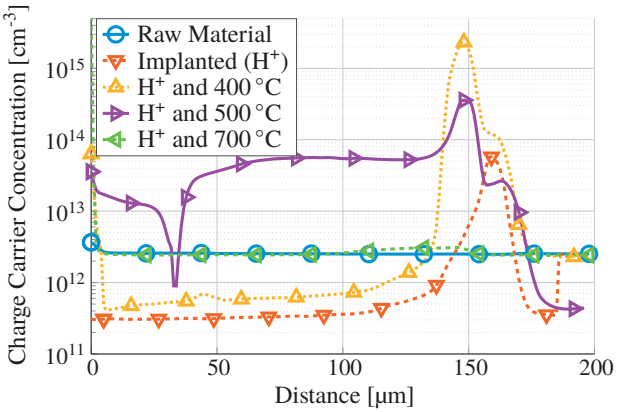

Figure 1 Charge carrier concentration profiles of the cross sections of silicon samples with different treatments. Proton implantation: 2×10^{14} H^+cm^{-2}, 4 MeV. Annealing time: 1 h. This figure has been generated from the data presented in reference [10].

2 Simulation method The simulation is based on the diffusion of point defects in the material and on their interaction with each other, forming defect complexes. It takes into account the diffusion of mobile defects, their reactions and dissociation, as well as the generation of new point defects during the implantation. The time dependent change of the concentration of a defect can be described by the equation

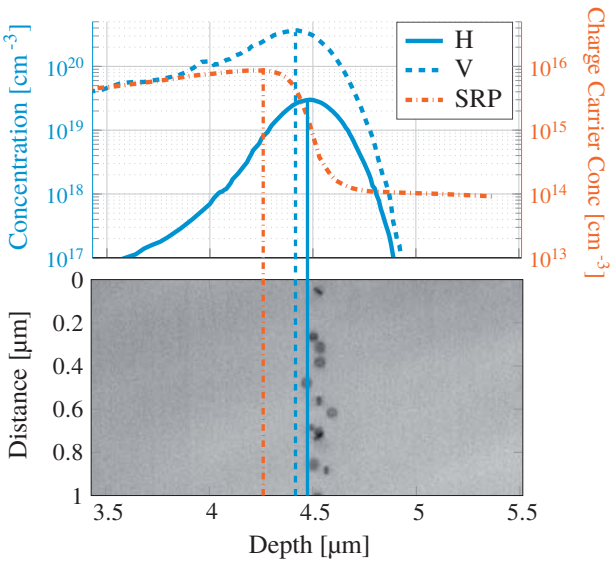

Figure 2 Investigation of a silicon sample implanted with a dose of 1×10^{15} H^+cm^{-2} 400 keV protons and annealed at 400 °C for 2 h. Top figure: Hydrogen (H) and vacancy (V) profiles simulated with SRIM and charge carrier concentration profile measured with SRP. Bottom figure: TEM image of extended defects. The vertical lines represent the depth of the concentration maxima in the top figure.

$$\frac{dc_n}{dt} = D_n\nabla^2 c_n + \sum_{lm} kp^n_{lm} c_l c_m - \sum_m ke^n_m c_n c_m - \\ - kd^m_n c_n + \sum_m ko^n_m c_m + c^G_n(t). \tag{8}$$

The first term of this equation describes the diffusion (see Eq. (1). The second term sums up all the reactions yielding the defect as a product. kp^n_{lm} is rate for the reaction of the defects l and m to n. The third term takes into account all the reactions where defect n is an educt, and hence, is consumed. ke^n_m represents the rate for the reaction of defect n and m to another defect. In the fourth term the dissociation of defect n to defect m is included. This is a first order reaction, whose rate kd^m_n is proportional to the concentration n. The dissociation of another defect, m, yielding defect n is accounted for in the next term and is described by the dissociation rate ko^n_m. $c^G_n(t)$ is the generation term. The only point defects which can be generated during proton implantation are hydrogen, vacancies and interstitials.

This formalism can be used at different levels of sophistication. Each charge state and each excited state and each lattice position of every point defect or complex can be treated as a separate defect, associated with diffusion and dissociation parameters, as well as, critical radii for reactions. In a first step of simplification one can average over the different excited states and only treat different charge states in the simulation. To simplify even further, one can average over the charge states and the exciting states.

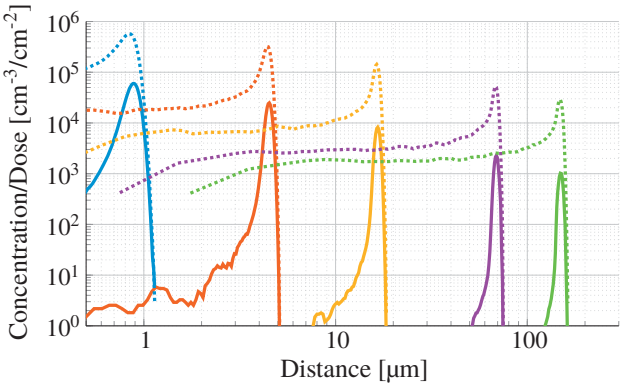

Figure 3 Log-log plot of point defect concentration profiles normalized to the proton dose ($\frac{c}{d}$) for different implantation energies simulated with SRIM. Solid lines: hydrogen, dashed lines: vacancies/interstitials. Simulated implantation energies (from left to right): 100 keV, 400 keV, 1 MeV, 2.5 MeV, 4 MeV. In the simulation an incidence angle of 7 ° was used.

2.1 Input While substitutional impurities are introduced as constant defect concentration profiles at the start of the simulation, hydrogen, vacancies and interstitials are introduced ($c^G_n(t)$) during the simulation. The introduced defect concentration profiles are simulated with SRIM. Figure 3 shows SRIM simulations of proton implantations into a silicon substrate for different implantation energies. The calculated defect concentrations are normalized to the implanted proton dose. As the kinetic energy of silicon atoms which are knocked from their lattice positions by hydrogen is rather small, they come to rest very close to their initial position in the lattice. Hence, the concentration profiles for vacancies and interstitials are assumed to coincide. The number of generated defects depends on the proton flux Φ:

$$\Phi = \frac{I}{eA}. \tag{9}$$

Here, I is the implantation current, A is the irradiated area and e is the elementary charge. During the proton implantation process the ion beam is scanned over the sample. Each point on the sample experiences a periodic generation of point defects as the beam is rastered. This introduces a time dependent generation $c^G_n(t)$ term in Eq. (8) . We modelled this with a delta pulse that repeats at the scan frequency f_{scan}. The integral over the delta pulse is the concentration

$$c_{\text{pulse}} = \left(\frac{c}{d}\right)_{\text{SRIM}} * \phi * f^{-1}_{\text{scan}}, \tag{10}$$

where $\left(\frac{c}{d}\right)_{\text{SRIM}}$ is the output of the SRIM simulation. At each pulse a high contraction of vacancies and interstitials is generated, many of which then react or annihilate before the next pulse generates new defects.

The simulation of the diffusion process at a certain temperature requires a diffusivity, which is calculated from Arrhenius coefficients (see Eq. (2)). Different charge states of the same defect often have different diffusivities. Depending on the level of sophistication, the diffusivity can be approximated by an effective diffusivity which averages over the diffusivities of the different charge states. Since the occupation of the charge states depends on the temperature (T) and the chemical potential (μ), this effective diffusion also depends on the temperature and the chemical potential. In a further step of simplification, the effective diffusivity could also average over different diffusion mechanisms, such as interstitial and vacancy mediated diffusion.

The reactions between the defects are approximated using diffusion limited second order reactions (see Eq. (3)). The rate of such a reaction is calculated according to Eq. (4) and depends on the diffusivities of the two educts and on the capture radius r_c. Most defect complexes can be formed through more than one reaction path. Each reaction path has a distinct capture radius. The capture radius is also a function of the chemical potential, since depending on μ, the reaction partners might have like or opposite charges. The Coulomb attraction results in an increased capture radius and Coulomb repulsion results in a decreased capture radius.

Defect complexes can also dissociate (see Eq. (7)). The dissociation depends on the charge state and the excited state of the dissociating defect.

2.2 Numerical solution To solve the implantation process numerically, Eq. (8) has to be discretized. The concentration change due to diffusion is calculated using the Backward-Euler method. The conversion of the reactions and dissociations are calculated for each spatial increment separately. New concentration profiles are calculated for $t + dt$ by adding the sum of the concentration changes to the initial defect concentration profiles. The time increment dt is a critical parameter. To ensure that the law of mass action is satisfied, dt is adjusted accordingly. The thermal generation of Frenkel-pairs (I and V) is not taken into account at this stage of the simulation, as at the examined process temperatures (lower than 200 °C) this effect is negligible.

3 Results An implantation process comprising 400 keV protons at a dose of 5×10^{14} H^+cm^{-2} at 100 °C was simulated using the method described above. The input data can be found in Table 1. The projected range of the protons at this energy is approximately 4.5 µm. The simulation averages over the contribution of different charge states and excited states. Changes of the chemical potential have not been taken into account. Table 2 gives an overview of Arrhenius parameters for the temperature activated diffusion of mobile defects used in this simulation. All defects which are not mentioned in Table 2 were considered to be immobile.

Table 1 Input data for the simulation.

Parameter	Input
Energy [kev]	400
Incidence angle [°]	7
Dose [H^+cm^{-2}]	5×10^{14}
Temperature [°C]	100
Flux [$H^+cm^{-2}s^{-1}$]	3.9×10^{11}
[B_s] [cm^{-3}]	1×10^{13}
[C_s] [cm^{-3}]	1×10^{16}
[O] [cm^{-3}]	2×10^{17}

Table 2 Arrhenius coefficients for the temperature activated diffusion for mobile defects in proton implanted silicon.

Defect	D_0 [cm^2/s]	$E_{A,diff}$ [eV]	Ref.
B_i	4.0×10^{-4}	0.6	[11]
C_i	4.4	0.88	[11]
H	3.3	1.22	[12]
H_2	7.4×10^{-4}	0.81	[13]
I	1.1×10^{-6}	0.12	[14]
I_2	3.8×10^{-1}	1.52	[15]
O	3.3×10^{-1}	2.59	[13]
O_2	2.3×10^{-2}	2.05	[13]
V	3.9×10^{-4}	0.3	[16]
V_2	3.0×10^{-3}	1.3	[17]

Table 3 Capture radii for a set of defect reactions found in Ref. [18].

Defect Reaction	r_c [Å]	Defect Reaction	r_c [Å]
$I + V \rightarrow$ annihilation	2	$B_s + I \rightarrow B_i$	2
$B_i + B_s \rightarrow B_iB_s$	20	$C_s + I \rightarrow C_i$	2
$B_i + O \rightarrow B_iO$	2	$V + V \rightarrow V_2$	2
$C_i + C_s \rightarrow C_iC_s$	4	$C_i + O \rightarrow C_iO$	4
$B_i + C_s \rightarrow B_iC_s$	40	$V + B_i \rightarrow B_s$	2
$C_i + C_iC_s \rightarrow C_{i2}C_s$	3	$V + O \rightarrow VO$	2
$B_i + B_iB_s \rightarrow B_{i2}B_s$	3	$V + C_i \rightarrow C_s$	2

Capture radii for a set of reactions can be found in Ref. [18] and are shown in Table 3. All other capture radii in this simulation have been assumed to be 2 Å.

The coefficients for the thermally activated dissociation can be found in Table 4. Most defect complexes containing hydrogen are assumed to dissociate. Unfortunately no kinetic parameters for this process have been found in literature, so the simulation uses the parameters of the dissociation of P_sH (see Table 4) to approximate this process.

Figure 4 shows concentration profiles of the impurities (B, C, O) and the generated point defects (H, I and V). Each of these profiles sums up all profiles containing the speci-

Table 4 Arrhenius coefficients for the temperature activated dissociation for defects in proton implanted silicon.

Defect	f_A [s^{-1}]	$E_{A,diss}$ [eV]	Ref.
B_iH	2.8×10^{14}	1.28	[7]
B_sH	2.8×10^{14}	1.28	[7]
P_sH	1.0×10^{13}	1.32	[6]
I_2O	2.2×10^{10}	1	[19]

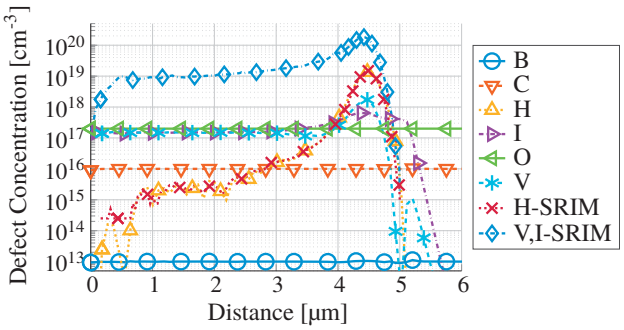

Figure 4 Concentration profiles of intrinsic point defects and point defects generated during a simulation of the proton implantation process using the input parameters in Table 1. The profiles show the sum of all defect profiles containing a certain point defect. Hydrogen and vacancy/interstitial profiles simulated with SRIM are added for comparison.

fied defect as a constituent. This assures, that the integrated concentration of the intrinsic defects has not been changed. Additionally the hydrogen- and vacancy/interstitial concentration profiles simulated with SRIM are shown. A high fraction of the vacancies and interstitials generated during the implantation immediately recombine and hence, annihilate. Both, direct and indirect recombination take place at the same time and decrease the concentration of intrinsic point defects obtained from SRIM by almost two orders of magnitude.

In Fig. 5 the actual concentration profiles of point defects after the implantation process are shown. The intrinsic point defects react quickly during the implantation. The oxygen concentration in the irradiated region is reduced by almost an order of magnitude and is even smaller at the implantation depth. Almost all substitutional carbon and boron defects have reacted. Small concentrations of interstitials and vacancies can be found, which are always present due to the equilibrium between reaction and dissociation of larger complexes. The interstitials spread deeper into the sample than the vacancies. In a region deeper than the projected range, a small peak of interstitial carbon can be observed. At the same position the concentrations of the intrinsic defects (B, C and O) return to their initial values. A high number of different defect complexes are formed during the proton implantation process. To allow for an easier

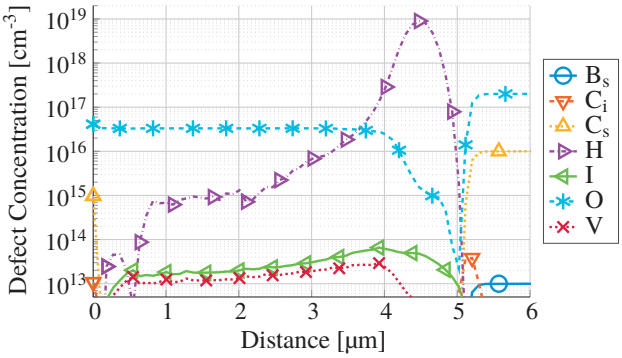

Figure 5 Concentration profiles of intrinsic and extrinsic point defects generated during a simulation of the proton implantation process using the input parameters in Table 1.

Table 5 Families of defect complexes. A selection of investigations on the corresponding defects can be found in the references.

Family	Defects	Refs.
B_i-complexes	B_i, B_iB_s, $B_{i2}B_s$, B_iC_s, B_iH, B_iH_2, B_iH_3, B_iO	[7,11,20]
C_i-complexes	C_i, C_iC_s, C_iC_sI, $C_iC_sI_2$, C_iH, C_iO, C_iOH, C_iOI, C_iOI_2	[11,21,22]
I-cluster	I-I_8	[11,23,24]
IO-complexes	IO,I_2O	[11,19,25]
OH-complexes	OH,OH_2	[26,27]
V-cluster	V-V_6	[11,28,29]
VOH-complexes	VH-VH_6,VOH, VOH_2, V_2H-V_2H_6, V_2OH	[30–32]
VO-complexes	VO-VO_3, V_2O-V_2O_3, V_3O-V_3O_3	[11,33,34]

interpretation of the defects which are formed, these defects were assigned to defect families. In Table 5 these families are listed. Their concentration profiles are shown in Fig. 6.

Most interstitials and vacancies which have not recombined, react with oxygen or hydrogen rather than to form clusters. While IO-complexes show a high concentration throughout the irradiated region and beyond the implantation depth, the concentration of VO-complexes is high in the irradiated region but decreases before the projected range. Around the implantation depth, most vacancies are found in VOH-defect complexes. A smaller fraction of the vacancies and interstitials forms clusters (V_n or I_n) and here, the concentration of interstitial clusters is higher than the concentration of vacancy clusters throughout the irradiated region and the implantation depth. H_2 and OH-complexes are localized around the implantation depth.

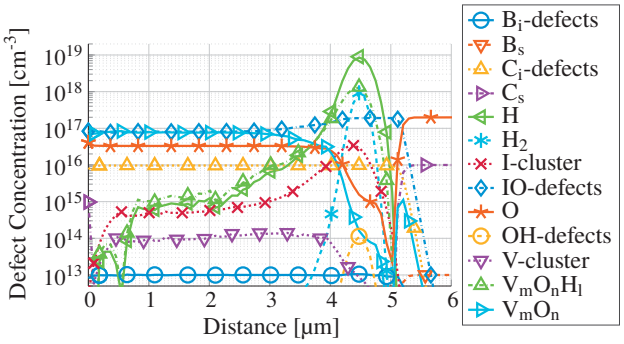

Figure 6 Concentration profiles of different defects and defect classes generated during a simulation of the proton implantation process using the input parameters in Table 1.

4 Conclusions A simulation for the generation of defect complexes during the proton implantation process is presented. It accounts for the diffusion, reaction and dissociation, as well as the generation of point defects and defect complexes. While many parameters used in the simulation are not yet known accurately, simulations such as the one presented here are useful for interpreting trends in the evolution of defects in silicon. The output of the proton implantation simulation is a set of defect concentration profiles which clearly show a reduction of the concentration of intrinsic point defects by almost two orders of magnitude compared to SRIM. Furthermore, the reduction of the concentrations of interstitial oxygen and substitutional impurities such as carbon and boron was at least an order of magnitude.

Acknowledgements This work has been performed in the project EPPL, co-funded by grants from Austria, Germany, The Netherlands, Italy, France, Portugal- ENIAC member States and the ENIAC Joint Undertaking. This project is co-funded within the program "Forschung, Innovation und Technologie für Informationstechnologie" by the Austrian Ministry for Transport, Innovation and Technology.

References

[1] P. Hazdra, K. Brand, J. Rubeš, and J. Vobeck, Microelectron. J. **32**(5), 449–456 (2001).
[2] Y. Zohta, Y. Ohmura, and M. Kanazawa, Jpn. J. Appl. Phys. **10**(4), 532 (1971).
[3] S. Romani and J. Evans, Nucl. Instrum. Methods B **44**(3), 313–317 (1990).
[4] M. von Smoluchowski, Z. Phys. **17**, 557–585 (1916).
[5] M. von Smoluchowski, Z. Phys. Chem. **92**, 129–168 (1917).
[6] K. Bergman, M. Stavola, S. Pearton, and J. Lopata, Phys. Rev. B **37**(5), 2770 (1988).
[7] T. Zundel and J. Weber, Phys. Rev. B **39**(18), 13549 (1989).
[8] J. Ziegler, SRIM(Version2013.00) - http://www.srim.org, 1984-2013.
[9] J. F. Ziegler, M. D. Ziegler, and J. P. Biersack, Nucl. Instrum. Methods B **268**(11), 1818–1823 (2010).
[10] M. Faccinelli, S. Kirnstoetter, W. Schustereder, J. G. Laven, and P. Hadley, Phys. Status Solidi C **11**(11-12), 1583–1588 (2014).
[11] P. Pichler, Intrinsic point defects, impurities, and their diffusion in silicon (Springer Science & Business Media, 2004).
[12] M. Capizzi and A. Mittiga, Physica B & C **146**(1), 19–29 (1987).
[13] V. Gusakov, Sol. Status Phenom. **205**, 171–180 (2014).
[14] V. Panteleev, S. Ershov, V. Chernyakhovskii, and S. Nagornykh, JETP Lett.+ **23**(12) (1976).
[15] M. Hane, T. Ikezawa, and G. H. Gilmer, International Conference on Simulation of Semiconductor Processes and Devices, 2000, SISPAD 2000, pp. 119–122 (2000).
[16] V. V. Voronkov and R. Falster, Sol. Status Phenom. **205**, 157–162 (2014).
[17] M. Mikelsen, E. Monakhov, G. Alfieri, B. Avset, and B. Svensson, Phys. Rev. B **72**(19), 195207 (2005).
[18] S. Zhao, Defect reactions and impurity control in silicon, PhD thesis, Massachusetts Institute of Technology, 1997.
[19] V. P. Markevich, A. R. Peaker, B. Hamilton, V. E. Gusakov, S. B. Lastovskii, L. I. Murin, N. Ganagona, E. Monakhov, and B. G. Svensson, Sol. Status Phenom. **242** (2016).
[20] J. Adey, R. Jones, and P. Briddon, Appl. Phys. Lett. **83**(4), 665–667 (2003).
[21] R. a. Pinacho, P. Castrillo, M. Jaraiz, I. Martin-Bragado, J. Barbolla, H. J. Gossmann, G. H. Gilmer, and J. L. Benton, J. Appl. Phys. **92**(3), 1582–1587 (2002).
[22] M. Potsidi and C. Londos, J. Appl. Phys. **100**(3), 033523 (2006).
[23] C. J. Ortiz, P. Pichler, T. Fühner, F. Cristiano, B. Colombeau, N. E. Cowern, and A. Claverie, J. Appl. Phys. **96**(9), 4866–4877 (2004).
[24] S. Libertino, S. Coffa, J. L. Benton, K. Halliburton, and D. J. Eaglesham, Nucl. Instrum. Methods B **148**(1), 247–251 (1999).
[25] N. Pinho, J. Coutinho, R. Jones, and P. Briddon, Physica B **340**, 575–577 (2003).
[26] V. Markevich and M. Suezawa, J. Appl. Phys. **83**(6), 2988–2993 (1998).
[27] R. Newman, J. Phys.: Condens. Mater **12**(25), R335(2000).
[28] S. Chakravarthi and S. T. Dunham, J. Appl. Phys. **89**(9), 4758–4765 (2001).
[29] T. Staab, A. Sieck, M. Haugk, M. J. Puska, T. Frauenheim, and H. Leipner, Phys. Rev. B **65**(11), 115210 (2002).
[30] S. Z. Tokmoldin and B. Mukashev, Physica B **308**, 167–170 (2001).
[31] M. Budde, B. B. Nielsen, J. Keay, and L. Feldman, Physica B **273**, 208–211 (1999).
[32] S. Estreicher, J. Hastings, and P. Fedders, Mater. Sci. Eng. B **58**(1), 31–35 (1999).
[33] J. Evans-Freeman, P. Kan, and N. Abdelgader, J. Appl. Phys. **92**(7), 3755–3760 (2002).
[34] G. Watkins and J. Corbett, Phys. Rev. **121**(4), 1001 (1961).